

High-precision photometry by telescope defocussing. I. The transiting planetary system WASP-5*

John Southworth^{1†}, T. C. Hinse^{2,3}, U. G. Jørgensen², M. Dominik^{4‡}, D. Ricci⁵,
M. J. Burgdorf⁶, A. Hornstrup⁷, P. J. Wheatley¹, T. Anguita⁸, V. Bozza^{9,10},
S. Calchi Novati^{9,10}, K. Harpsøe², P. Kjærgaard², C. Liebig⁸, L. Mancini^{9,10},
G. Masi¹¹, M. Mathiasen², S. Rahvar¹², G. Scarpetta^{9,10}, C. Snodgrass¹³,
J. Surdej⁵, C. C. Thöne^{14,15}, M. Zub⁸

¹ *Department of Physics, University of Warwick, Coventry, CV4 7AL, UK*

² *Niels Bohr Institute, University of Copenhagen, Juliane Maries Vej 30, Copenhagen Ø, 2100, Denmark*

³ *Armagh Observatory, College Hill, Armagh, BT61 9DG, Northern Ireland, UK*

⁴ *SUPA, University of St Andrews, School of Physics & Astronomy, North Haugh, St Andrews, KY16 9SS, UK*

⁵ *Institut d'Astrophysique et de Géophysique, Université de Liège, 4000 Liège, Belgium*

⁶ *Astrophysics Research Institute, Liverpool John Moores University, Twelve Quays House, Egerton Wharf, Birkenhead, CH41 1LD, UK*

⁷ *National Space Institute, Technical University of Denmark, Juliane Maries Vej 30, Copenhagen Ø, 2100, Denmark*

⁸ *Astronomisches Rechen-Institut, Zentrum für Astronomie, Universität Heidelberg, Mönchhofstrasse 12-14, 69120 Heidelberg, Germany*

⁹ *Dipartimento di Fisica "E. R. Caianiello", Università di Salerno, Baronissi, Italy*

¹⁰ *Istituto Nazionale di Fisica Nucleare, Sezione di Napoli, Italy*

¹¹ *Bellatrix Observatory, Centre for Backyard Astrophysics, Ceccano (FR), Italy*

¹² *Sharif University of Technology, Tehran, Iran*

¹³ *European Southern Observatory, Casilla 19001, Santiago 19, Chile*

¹⁴ *Dark Cosmology Centre, Niels Bohr Institute, University of Copenhagen, Juliane Maries Vej 30, Copenhagen Ø, 2100, Denmark*

¹⁵ *INAF, Osservatorio Astronomico di Brera, 23807 Merate, Italy*

12 March 2009

ABSTRACT

We present high-precision photometry of two transit events of the extrasolar planetary system WASP-5, obtained with the Danish 1.54 m telescope at ESO La Silla. In order to minimise both random and flat-fielding errors, we defocussed the telescope so its point spread function approximated an annulus of diameter 40 pixels ($16''$). Data reduction was undertaken using standard aperture photometry plus an algorithm for optimally combining the ensemble of comparison stars. The resulting light curves have point-to-point scatters of 0.50 mmag for the first transit and 0.59 mmag for the second. We construct detailed signal to noise calculations for defocussed photometry, and apply them to our observations. We model the light curves with the JKTEBOP code and combine the results with tabulated predictions from theoretical stellar evolutionary models to derive the physical properties of the WASP-5 system. We find that the planet has a mass of $M_b = 1.637 \pm 0.075 \pm 0.033 M_{\text{Jup}}$, a radius of $R_b = 1.171 \pm 0.056 \pm 0.012 R_{\text{Jup}}$, a large surface gravity of $g_b = 29.6 \pm 2.8 \text{ m s}^{-2}$ and a density of $\rho_b = 1.02 \pm 0.14 \pm 0.01 \rho_{\text{Jup}}$ (statistical and systematic uncertainties). The planet's high equilibrium temperature of $T_{\text{eq}} = 1732 \pm 80 \text{ K}$, makes it a good candidate for detecting secondary eclipses.

Key words: stars: planetary systems — stars: individual: WASP-5 — stars: binaries: eclipsing — methods: data analysis — methods: observational — techniques: photometric

1 INTRODUCTION

The discovery of the first extrasolar planet (Mayor & Queloz 1995) opened a new field of astronomical research. We now

* Based on data collected by MiNDSTeP with the Danish 1.54 m telescope at the ESO La Silla Observatory

† E-mail: j.k.taylor@warwick.ac.uk

‡ Royal Society University Research Fellow

know of over 300 extrasolar planets¹, which encourages statistical studies of these objects (e.g. Udry & Santos 2007). However, most of these discoveries have been made via measurements of the radial velocities of their parent stars, which yield relatively little information about individual planets (only the orbital parameters and lower limits on the planet's mass).

The discovery of transiting extrasolar planets (hereafter TEPs) in the year 1999 (Charbonneau et al. 2000; Henry et al. 2000) has provided a new window on the properties of extrasolar gas-giant planets, making it possible to derive the physical properties of planets and their parent stars (with a little help from stellar theory). These analyses require high-precision photometry of planetary transits in order to measure the radii of the components and the inclination of their orbital plane with respect to Earth.

Good light curves have been obtained for a substantial number of the roughly fifty known TEPs, but the process remains fraught with difficulties. Ground-based studies are subject to complications arising due to scintillation, atmospheric effects which change throughout transit observations, telescope tracking errors, and problems with saturation and flat-fielding of the ubiquitous charge-coupled device (CCD) detectors. Space-based facilities, however, can be subject to major cost and calibration issues.

We have therefore decided to experiment with heavy defocussing of ground-based telescopes in order to nullify as many as possible of the above effects. The idea is to choose relatively long integration times (several minutes) and disperse the resulting large numbers of photons over many CCD pixels. This has the huge advantage that flat-fielding errors can be averaged down by orders of magnitude compared to focussed observations, and also means that normal changes in atmospheric seeing are irrelevant. Nonlinear pixel responses should be corrected by calibrating the response of the CCD or avoided by sticking to count levels where such effects are low. The longer integration times and large point spread functions (PSFs) mean that the sky background level is much higher than for standard approaches, but signal-to-noise calculations (Section 6) show that this is unimportant in many cases.

In this work we present high-precision photometry of WASP-5, a $V = 12.3$ star which was discovered to harbour a TEP by Anderson et al. (2008). We used the Danish 1.54 m telescope at ESO La Silla, Chile, as part of the 2008 MiNDSTeP campaign², and the DFOSC imaging camera. It was suspected that DFOSC would not be suited to these observations, as focal-reducing instruments can suffer internal reflections, but this does not appear to be a problem. We observed two transit events and achieved observational scatters of only 0.50 mmag and 0.59 mmag per point in the final light curves. In the following sections we discuss our observations and data reduction procedures, and then analyse the data using the methods detailed by Southworth (2008, 2009). Our results are fully homogeneous with those of the

fourteen TEPs analysed in these papers, and represent the highest-precision measurements of the physical properties of the star and planet in the WASP-5 system.

Whilst it is unusual to break the 1 mmag barrier in astronomical differential photometry, our observations do not set any records. Gilliland et al. (1993) obtained observational scatters of 0.25 mmag per minute in time-series observations of stars in the open cluster M67. These authors used a set of 4m-class telescopes, allowing them to achieve a lower Poisson and scintillation noise than ourselves, and CCD imagers with much finer pixel scale, which meant much less defocussing and so a lower sky background.

A number of researchers have used some telescope defocussing to improve the photometric accuracy of light curves of TEPs, in many cases broadening the PSFs by only a few pixels. A partial list includes studies of GJ 436 (Gillon et al. 2007; Demory et al. 2007; Alonso et al. 2008), HD 17156 (Gillon et al. 2008a), HD 189733 (Winn et al. 2007a), HAT-P-1 (Winn et al. 2007b), *Hubble Space Telescope* observations of HD 189733 (Swain et al. 2008), and the NASA EPOXI mission (Christiansen et al. 2008). The discovery paper of WASP-5 (Anderson et al. 2008) presented a light curve from a 1.2 m telescope which achieved a scatter of about 1 mmag using this technique. Substantial defocussing was also used by Gillon et al. (2008b) in the course of obtaining a light curve of WASP-5 using the VLT, but the resulting data suffer systematic effects which were not removable. These were attributed to deformation of the primary mirror, as the active optics had to be turned off to permit defocussing. Finally, PSF broadening has been performed both by moving the telescope during individual exposures (Bakos et al. 2004) and by shuffling charge at will round an orthogonal-transfer CCD device (Tonry et al. 2005; Johnson et al. 2008).

2 OBSERVATIONS

We observed two transits of WASP-5 using the 1.54 m Danish³ Telescope at ESO La Silla and the DFOSC focal-reducing imager. This setup yielded a full field of view of $13.7' \times 13.7'$ and a plate scale of $0.39'' \text{ pixel}^{-1}$. For the second set of observations the CCD was windowed down to approximately 2000×800 pixels to decrease the readout time from 91 s to 39 s. All observations were done through the Cousins R filter, which allowed a higher count rate than Johnson V for red stars but did not suffer the fringing effects visible with DFOSC and the Cousins I filter. An observing log is given in Table 1. The observing conditions and sky transparency were good throughout both nights.

The exposure time was set at 120 s, to allow a large amount of light to be collected in each observation whilst avoiding undersampling the light variations through transit (see Section 6 for detailed signal to noise calculations). We then adjusted the amount of defocussing until the peak counts per pixel from WASP-5 were roughly 25 000 above the sky background. This resulted in a doughnut-shaped

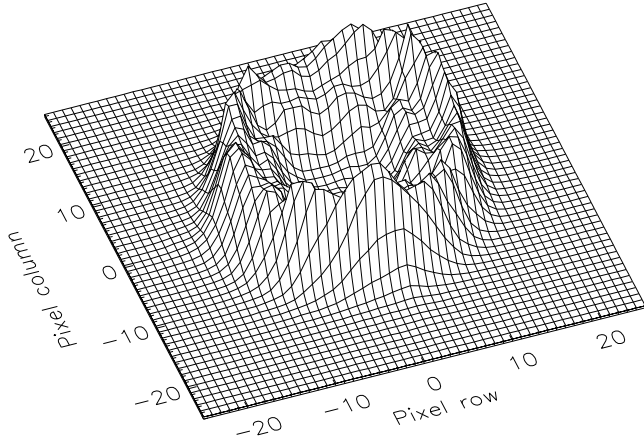
¹ See <http://exoplanet.eu/> for a list of known extrasolar planets.

² Information on the MiNDSTeP (Microlensing Network for the Detection of Small Terrestrial Exoplanets) campaign can be found at www.mindstep-science.org/

³ Information on the 1.54 m Danish Telescope and DFOSC can be found at <http://www.eso.org/sci/facilities/lasilla/telescopes/d1p5/>

Table 1. Log of the observations presented in this work.

Date	Start time (UT)	End time (UT)	Number of observations	Exposure time (s)	Airmass
2008 08 29	05:37	10:08	74	120.0	1.03–1.54
2008 09 21	01:06	05:32	101	120.0	1.03–1.40


Figure 1. Surface plot of the PSF of WASP-5 in an image taken at random from the observing sequence on the night of 2008 August 29th. The x and y axes are in pixels. The lowest and highest counts are 623 and 28429 ADUs, respectively, and the z axis is on a linear scale.

PSF with a diameter of about 40 pixels ($16''$) and containing roughly 10^7 counts from WASP-5. Once the amount of defocussing was settled on, it was not changed until the end of the observing sequence. An example PSF of WASP-5 is shown in Fig. 1.

A few images were also taken with the telescope properly focussed, and were used to verify that there were no faint stars within the PSF of WASP-5 which might dilute the transit depth. We found that the closest detectable star to WASP-5 is at a distance of $44''$ (113 pixels), so the edge of its PSF is separated from that of WASP-5 by over 70 pixels in our defocussed images. The closest stars of similar to or greater brightness than WASP-5 lie over $4'$ away. We conclude that no stars interfere with the PSF of WASP-5.

3 DATA REDUCTION

Our data reduction pipeline is written in the IDL⁴ programming language and uses the DAOPHOT photometry package (Stetson 1987) (distributed as part of the ASTROLIB⁵ library) to perform aperture photometry. The telescope was autoguided throughout our observations so it was possible to fix the positions of the circular apertures for each dataset. We experimented with different aperture radii, finding that this had a small effect on the scatter in the photometry but no

detectable effect on the shape of the resulting transits. We chose the apertures which yielded the most precise photometry, with radii of 28 pixels for the PSF and 38 and 60 pixels for the inner and outer edges of the sky regions, respectively. Thus a PSF aperture covered 2463 pixels and a sky region covered 6773 pixels.

We used these aperture sizes and the ASTROLIB/APER routine to obtain aperture photometry of all stars in our images with sufficient counts to be useful. The number of comparison stars was either eight or nine for these observations. The differential-magnitude light curves of all these stars were checked for short-timescale variability, and none was found. Most of the comparison star light curves have slow variations in their apparent brightness, attributable to atmospheric effects, so variability on timescales greater than about 5 hr would not be detectable.

To remove these slow variations in the differential-magnitude light curves we implemented an algorithm to optimise the selection of comparison stars. We defined time intervals outside transit and used the IDL/AMOEBA routine to minimise the square of the magnitude values within these intervals, resulting in light curves which were normalised to zero differential magnitude. The parameters of the minimisation were N coefficients of a polynomial versus time, and weights of each comparison star relative to the first comparison star. All good comparison stars were combined into one ensemble by weighted flux summation. For each dataset we used $N = 2$, which removes overall variations without deforming the shape of the transit. We found that it was necessary to have $N > 1$ because we have too few comparison stars to create an ensemble with a low Poisson noise and the same photometric colour as the target star. We found that the best-fitting comparison star weights were usually close to unity, as expected for observations dominated by Poisson noise.

Finally, we experimented with the inclusion of bias and flat-field corrections to the science images. Master bias and flat field images were created by median-combining sets of bias images and dome flats. We found that subtraction of a master bias image had a negligible effect on the photometry, as the bias level of the DFOSC CCD is well-behaved and exhibits minimal changes which are simply subsumed into the estimation of the sky background. Including a flat-fielding correction, however, gives a small but noticeable decrease in the scatter of the resulting light curves. The flat-fielding is relatively unimportant in this case because the stellar PSFs were kept on the same pixels by autoguiding the telescope. We have applied bias and flat-field corrections to generate our final light curves, which are shown in Fig. 2 and reproduced in Table 2.

4 LIGHT CURVE MODELLING

Southworth (2008, 2009) presented an homogeneous analysis of fourteen well-observed TEPs. We have used the same methods here, so our findings are fully compatible with the results in these papers. The analysis splits naturally into two steps, the first of which is modelling the light curves (Southworth 2008), and the second of which is including additional observed quantities to determine the physical properties of the star and planet (Southworth 2009).

⁴ The acronym IDL stands for Interactive Data Language and is a trademark of ITT Visual Information Solutions. For further details see <http://www.itervis.com/ProductServices/IDL.aspx>.

⁵ The ASTROLIB subroutine library is distributed by NASA. For further details see <http://idlastro.gsfc.nasa.gov/>.

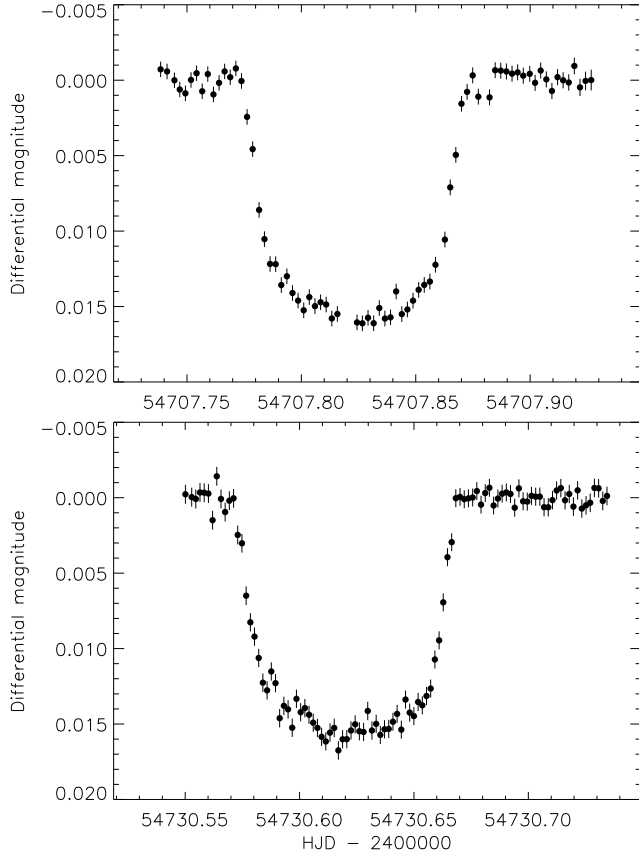


Figure 2. Final light curves of WASP-5 from our two nights of observations. The observational error bars were too conservative so have been shrunk to match the scatter of the data.

Table 2. Excerpts of the light curve of WASP-5. The full dataset will be made available in the electronic version of this paper and at the CDS.

HJD	Differential magnitude	Uncertainty
2454707.739980	−0.000722	0.000512
2454707.742816	−0.000580	0.000513
2454707.746034	0.000004	0.000512
2454707.748360	0.000616	0.000512
2454707.750814	0.000870	0.000513
2454730.554371	−0.000038	0.000630
2454730.556153	0.000084	0.000629
2454730.557982	−0.000347	0.000628
2454730.559811	−0.000330	0.000627
2454730.561651	−0.000274	0.000625

The transit light curves of WASP-5 were modelled using the JKTEBOP⁶ code (Southworth et al. 2004a,b), which is based on the EBOP program originally developed for eclipsing binary star systems (Popper & Etzel 1981; Etzel 1981; Nelson & Davis 1972). The parameters of the fit include the fractional radii of the star and planet, which are directly dependent on the shape of the light curve and are defined to

be $r_A = \frac{R_A}{a}$ and $r_b = \frac{R_b}{a}$ where R_A and R_b are the absolute radii of the components and a is the orbital semimajor axis. The fractional radii are actually parameterised as $r_A + r_b$ and $k = \frac{r_A}{r_b}$ in JKTEBOP, as these are only weakly correlated with each other (Southworth 2008). The other ‘shape’ parameters are the orbital inclination, i , and the limb darkening coefficients of the star, u_A and v_A (see below). The mass ratio of the system is also a parameter as it affects the shapes of the components. We adopted a value of 0.00155, and verified that large changes in this number had a negligible effect on our results.

The main analysis of our photometry was undertaken before any transit timings were available in the literature. We therefore allowed the midpoints of the two eclipses to float freely, by including the orbital period and eclipse midpoint as fitted parameters, to guard against possible period. We have also modelled the two light curves individually to measure two times of minimum light: $2454707.82388 \pm 0.00029$ and $2454730.62115 \pm 0.00032$ (HJD). During this process we found that the error bars in our data (which come from the IDL/APER routine) are slightly conservative and result in reduced χ^2 values of $\chi_{\text{red}}^2 = 0.95$ and 0.75 for the two datasets. We therefore multiplied the error bars by $\sqrt{\chi_{\text{red}}^2}$ before combining the data from the two nights into one light curve (see e.g. Bruntt et al. 2006).

Our two times of minimum light have been augmented with the four transit times given by Gillon et al. (2008b) and used to determine a linear ephemeris. Gillon et al. found that a straight line was not a good representation of the data ($\chi_{\text{red}}^2 = 5.7$). With our additional data we can associate this discrepancy with the transit time from their FTS light curve, which is earlier by 3σ that predicted by our linear ephemeris. Further data are needed to decide whether the cause is astrophysical or observational. Using all times of minimum light, we find

$$T_0 = \text{HJD}2454375.62494(24) + 1.6284246(13) \times E$$

where quantities in parentheses denote the uncertainty in the final digit of the preceding number.

In Southworth (2008) it was found that the treatment of the stellar limb darkening (LD) requires careful thought. LD is included in JKTEBOP as a choice of several parametric ‘laws’ for which coefficients must be specified. The linear law is inadequate for high-precision observations, whereas more sophisticated nonlinear laws suffer from strong correlations between their coefficients (Southworth et al. 2007a; Southworth 2008). Furthermore, theoretically calculated LD coefficients depend on stellar model atmospheres and do not match the highest-quality observations. The solution is to adopt nonlinear laws but to fix one of the coefficients at a reasonable value. An alternative would be to re-parameterise the two-coefficient laws so the coefficients have weaker correlations, but this has little effect on the other parameters of the fit.

We have incorporated LD using the linear, quadratic, square-root, logarithmic or cubic laws. We present one set of solutions where both the linear (u_A) and nonlinear (v_A) LD coefficients are fixed to theoretical values (Table 3). We also give a set of solutions where u_A is a fitted parameter and v_A is fixed to theoretical values (Table 4). In the second case, v_A is perturbed by ± 0.1 on a flat distribution during the error analysis. The theoretical LD coefficients are taken to be the

⁶ JKTEBOP is written in FORTRAN77 and the source code is available at <http://www.astro.keele.ac.uk/~jkt/>

Table 3. Parameters of the JKTEBOP best fits of the light curve of WASP-5 for different LD laws with the coefficients fixed at theoretically predicted values. For each part of the table the upper quantities are fitted parameters and the lower quantities are derived parameters. Results were not calculated using the cubic LD law because theoretical LD coefficients are not available.

	Linear LD law	Quadratic LD law	Square-root LD law	Logarithmic LD law
$r_A + r_b$	0.2036 ± 0.0056	0.2009 ± 0.0057	0.2085 ± 0.0050	0.2024 ± 0.0057
k	0.1103 ± 0.0010	0.1096 ± 0.0010	0.1119 ± 0.0007	0.1100 ± 0.0009
i (deg.)	86.17 ± 0.84	86.66 ± 0.96	85.37 ± 0.60	86.37 ± 0.90
u_A	0.60 fixed	0.40 fixed	0.20 fixed	0.70 fixed
v_A		0.30 fixed	0.50 fixed	0.20 fixed
r_A	0.1834 ± 0.0048	0.1811 ± 0.0051	0.1875 ± 0.0044	0.1824 ± 0.0050
r_b	0.02022 ± 0.00071	0.01984 ± 0.00070	0.02098 ± 0.00061	0.02006 ± 0.00071
σ (mmag)	0.5696	0.5593	0.5586	0.5602

Table 4. Parameters of the JKTEBOP best fits of the light curve of WASP-5 for different LD laws with the linear coefficients included as fitted parameters and the nonlinear coefficients fixed at theoretically predicted values which are perturbed in the Monte Carlo error analysis. For each part of the table the upper quantities are fitted parameters and the lower quantities are derived parameters.

	Linear LD law	Quadratic LD law	Square-root LD law	Logarithmic LD law	Cubic LD law
$r_A + r_b$	0.2097 ± 0.0052	0.2034 ± 0.0062	0.2058 ± 0.0053	0.2054 ± 0.0056	0.2059 ± 0.0060
k	0.1125 ± 0.0009	0.1102 ± 0.0013	0.1112 ± 0.0011	0.1110 ± 0.0011	0.1114 ± 0.0012
i (deg.)	85.16 ± 0.64	86.22 ± 1.02	85.77 ± 0.75	85.83 ± 0.77	85.73 ± 0.81
u_A	0.508 ± 0.031	0.378 ± 0.048	0.227 ± 0.049	0.659 ± 0.058	0.495 ± 0.037
v_A		0.30 perturbed	0.50 perturbed	0.20 perturbed	0.10 perturbed
r_A	0.1885 ± 0.0046	0.1832 ± 0.0055	0.1852 ± 0.0047	0.1849 ± 0.0049	0.1852 ± 0.0052
r_b	0.02119 ± 0.00067	0.02019 ± 0.00083	0.02058 ± 0.00070	0.02053 ± 0.00071	0.02063 ± 0.00077
σ (mmag)	0.5576	0.5579	0.5578	0.5579	0.5578

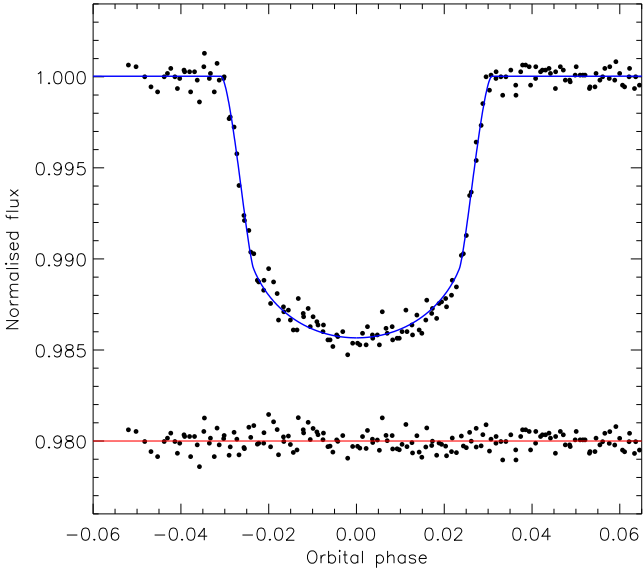


Figure 3. Phased light curve of the two transits of WASP-5 compared to the best fit found using JKTEBOP and the quadratic LD law with both LD coefficients included as fitted parameters. The residuals of the fit are plotted at the bottom of the figure, offset from zero.

approximate mean of values found by bilinear interpolation within the tabulations of Van Hamme (1993), Claret (2000, 2004a) and Claret & Hauschildt (2003).

We have used Monte Carlo simulations to assign uncer-

tainties to the parameters found from the light curve, following the procedures of Southworth et al. (2004b, 2005b). Each fit was followed by 1000 Monte Carlo simulations and 1σ error bars were calculated from the scatter in the simulation results (Tables 3 and 4). This does not account for any systematic errors which might be in our light curves, so this possibility was investigated using the residual-permutation approach (Jenkins et al. 2002) and found to be marginally significant. The residuals in Fig. 3 suggest there are minor systematic effects, in agreement with the residual-permutation results.

From Tables 3 and 4 it can be seen that the solutions with LD coefficients fixed at theoretical values have slightly larger residuals than those where the linear LD coefficient is a parameter of the fit. We have therefore used the latter solutions for our final results, combined following the methods of Southworth (2008) and incorporating the systematic uncertainties found with the residual-bead method. The final values of the photometric parameters are given in Table 5. They are in agreement with and more precise than the values found in the two previous studies of WASP-5, Anderson et al. (2008) and Gillon et al. (2008b), which used the same photometric data. Including the stellar velocity amplitude given by Anderson et al. (2008), we measure the surface gravity of the planet to be $g_b = 29.6 \pm 2.8 \text{ m s}^{-2}$ (see Southworth et al. 2007b).

Table 5. Final parameters of the fit to the light curve of WASP-5, based on the individual solutions given in Table 4. The orbital ephemeris was determined separately (Section 4). The results of Anderson et al. (2008) and Gillon et al. (2008b), which are based on the same photometric data, are included for comparison, and are without error bars if they were not directly quoted quantities. T_0 is the reference time of mid-transit.

	This work	Anderson et al. (2008)	Gillon et al. (2008b)
Orbital period (d)	1.6284246 ± 0.0000013	$1.6284296^{+0.0000048}_{-0.0000037}$	$1.6284279^{+0.0000022}_{-0.0000049}$
T_0 (HJD)	$2454375.62494 \pm 0.00024$	$2454375.62466^{+0.00026}_{-0.00025}$	$2454373.99598^{+0.00025}_{-0.00019}$
$r_A + r_b$	0.2052 ± 0.0068	0.197	0.198
k	0.1110 ± 0.0014	$0.1092^{+0.0030}_{-0.0017}$	$0.1086^{+0.0010}_{-0.0013}$
i ($^\circ$)	85.8 ± 1.1	85.0 to 90.0	$86.9^{+2.8}_{-0.7}$
r_A	0.1847 ± 0.0061	0.178	0.179
r_b	0.02050 ± 0.00091	0.0194	0.0194

5 PHYSICAL PROPERTIES OF WASP-5

The photometric parameters determined above have been used to infer the physical properties of the WASP-5 system using the method outlined in Southworth (2009). It is not possible to calculate the properties directly from observations, as one piece of information is missing and must be filled in by additional constraints. This approach requires as input the measured values of r_A , r_b , i , orbital period, and the stellar effective temperature, metallicity and velocity amplitude. For the latter three quantities we adopted $T_{\text{eff}} = 5700 \pm 100$ K and $[\frac{M}{H}] = 0.09 \pm 0.09$ dex from Gillon et al. (2008b) and $K_A = 278 \pm 8$ km s $^{-1}$ from Anderson et al. (2008). We then interpolated within the tabulated predictions of several sets of theoretical stellar models to provide the optimum fit to the input quantities. The stellar models used were Claret (Claret 2004b, 2005, 2006, 2007), Y^2 (Demarque et al. 2004) and Padova (Girardi et al. 2000). The uncertainties in the input parameters were propagated into the output physical properties using a perturbation analysis (Southworth 2009; Southworth et al. 2005a), which allows a detailed error budget to be obtained for each output quantity.

The use of theoretical stellar model predictions means that the calculated physical properties of the WASP-5 system are subject to systematic errors caused by any deviations of the models from reality. Unfortunately, stellar models are persistently unable to match the directly measured physical properties of low-mass eclipsing binary star systems, although this effect is likely due to magnetic activity (Hoxie 1973; Clausen 1998; Torres & Ribas 2002; Ribas et al. 2008). A lower limit can be set on the systematic errors by considering the variation in results from different sets of stellar models. This is only a lower limit because independent models have some physical ingredients in common, for example opacity tables. A probable upper limit can be set by avoiding stellar models and instead constraining the properties using an empirical main-sequence mass–radius relation for the star (Southworth 2009). Table 6 contains the physical properties of WASP-5 calculated using the three different sets of stellar models and with the mass–radius relation.

The properties calculated using stellar models are in good agreement with each other, whereas those determined using the mass–radius relation are offset to larger values. The difference is most significant for the orbital semimajor

Table 7. Detailed error budget for the calculation of the physical properties of the WASP-5 system from the light curve parameters, stellar velocity amplitude, and the predictions of the Claret stellar models. Each number in the table is the fractional contribution to the final uncertainty of an output parameter from the error bar of an input parameter. The final uncertainty for each output parameter (not given) is the quadrature sum of the individual contributions from each input parameter. P represents the orbital period.

Output parameter	P	K_A	Input parameter				
			i	r_A	r_b	T_{eff}	$[\frac{M}{H}]$
Age				0.341		0.753	0.556
a		0.001		0.075		0.760	0.644
M_A				0.075		0.760	0.645
R_A				0.871		0.374	0.317
$\log g_A$				0.967		0.195	0.166
ρ_A				1.000			
M_b		0.627	0.031	0.059		0.592	0.502
R_b				0.028	0.927	0.284	0.241
g_b		0.307	0.015		0.951		
ρ_b		0.208	0.010	0.010	0.969	0.099	0.083

axis (a) and the stellar mass (M_A) as these quantities are quite affected by systematics but almost unaffected by observational uncertainties. The error budget for the output parameters is given in Table 7, and shows that more precise stellar T_{eff} and $[\frac{M}{H}]$ measurements would be useful, as well as further high-precision photometry.

Table 8 gives the final physical properties for WASP-5, with statistical errors obtained from the perturbation analysis and systematic errors from consideration of the inter-agreement between results calculated using the three different sets of stellar evolutionary models. We have adopted the values of the properties obtained using the Claret models, in order to retain homogeneity with the analyses of Southworth (2009). A comparison with the results of Anderson et al. (2008) and Gillon et al. (2008b) shows that all quantities agree within the quoted uncertainties. The main difference is that our more extensive photometry yields a larger radius and thus a lower density for the planet; this arises from the light curve analysis via the parameter r_b .

Table 6. Physical properties for WASP-5, derived using either an empirical stellar mass–radius relation or the predictions of different sets of stellar evolutionary models. The stellar mass, radius, surface gravity and density are denoted by M_A , R_A , $\log g_A$ and ρ_A , respectively.

		Mass–radius	Padova models	Y ² models	Claret models
a	(AU)	0.02777 ± 0.00078	0.02702 ± 0.00046	0.02728 ± 0.00043	0.02729 ± 0.00049
M_A	(M_\odot)	1.076 ± 0.091	0.991 ± 0.051	1.020 ± 0.048	1.021 ± 0.055
R_A	(R_\odot)	1.103 ± 0.060	1.073 ± 0.039	1.083 ± 0.040	1.084 ± 0.039
$\log g_A$	[cgs]	4.385 ± 0.024	4.373 ± 0.030	4.377 ± 0.029	4.377 ± 0.030
ρ_A	(ρ_\odot)	0.803 ± 0.080	0.803 ± 0.080	0.803 ± 0.080	0.803 ± 0.080
M_b	(M_{Jup})	1.70 ± 0.11	1.604 ± 0.073	1.635 ± 0.070	1.637 ± 0.075
R_b	(R_{Jup})	1.191 ± 0.063	1.159 ± 0.055	1.170 ± 0.055	1.171 ± 0.056
g_b	(m s^{-2})	29.6 ± 2.7	29.6 ± 2.8	29.6 ± 2.8	29.6 ± 2.8
ρ_b	(ρ_{Jup})	1.00 ± 0.14	1.03 ± 0.14	1.02 ± 0.14	1.02 ± 0.14
Age	(Gyr)		$6.6^{+1.9}_{-3.3}$	$5.9^{+2.2}_{-1.9}$	$6.8^{+3.0}_{-2.5}$

Table 8. Final physical properties for WASP-5. The first error bars are statistical and the second are systematic. The corresponding results from Anderson et al. (2008) and Gillon et al. (2008b) have been included for comparison.

		Final result (this work)	Anderson et al. (2008)	Gillon et al. (2008b)
a	(AU)	$0.02729 \pm 0.00049 \pm 0.00027$	$0.02683^{+0.00088}_{-0.00075}$	$0.0267^{+0.0012}_{-0.0008}$
M_A	(M_\odot)	$1.021 \pm 0.055 \pm 0.030$	$0.972^{+0.099}_{-0.079}$	$0.96^{+0.13}_{-0.09}$
R_A	(R_\odot)	$1.084 \pm 0.040 \pm 0.011$	$1.026^{+0.073}_{-0.044}$	$1.029^{+0.056}_{-0.069}$
$\log g_A$	[cgs]	$4.377 \pm 0.030 \pm 0.004$	$4.403^{+0.039}_{-0.048}$	$4.395^{+0.043}_{-0.040}$
ρ_A	(ρ_\odot)	$0.803 \pm 0.080 \pm 0.000$	0.90	0.88 ± 0.12
M_b	(M_{Jup})	$1.637 \pm 0.075 \pm 0.033$	$1.58^{+0.13}_{-0.08}$	$1.58^{+0.13}_{-0.10}$
R_b	(R_{Jup})	$1.171 \pm 0.056 \pm 0.012$	$1.090^{+0.094}_{-0.058}$	$1.087^{+0.068}_{-0.071}$
g_b	(m s^{-2})	29.6 ± 2.8	$30.5^{+3.2}_{-4.1}$	$30.5^{+4.0}_{-2.9}$
ρ_b	(ρ_{Jup})	$1.02 \pm 0.14 \pm 0.01$	$1.22^{+0.19}_{-0.24}$	$1.23^{+0.26}_{-0.16}$

6 WHAT IS THE OPTIMAL EXPOSURE TIME?

Having presented and interpreted our observations, we now present detailed signal to noise (S/N) calculations which can be used to plan similar projects. The output quantities include the amount of defocussing required, and the total noise to signal ratio in millimagnitudes. The tractability of these calculations demands several approximations, so the results should not be overinterpreted. The IDL code used for the calculations can be obtained from the first author.

The important point here is that the quantity of interest for a given observing sequence is the achievable S/N *per unit time* rather than per observation. This is limited in particular by CCD readout for short exposures and sky background noise for long integrations. There will be an optimum value between these two extremes, which depends on the target and observing facilities.

We start with count rates for the target (overall) and for the sky background (per pixel) gathered from the SIGNAL⁷ code. These are appropriate for the Isaac Newton Telescope and Wide Field Camera, so must be scaled for the difference in telescope aperture (1.5 m versus 2.5 m) and plate scale ($0.39'' \text{ pixel}^{-1}$ instead of $0.33'' \text{ pixel}^{-1}$). We adopt the default values for sky brightness in dark, grey and bright time; this approximation can be improved as and when ad-

ditional information is available. The count rates are specified in electrons, so the CCD gain level is taken into account with the input parameters rather than as part of the S/N calculations.

For a given t_{exp} (in seconds) we calculate the total electrons obtained from the target, and the associated Poisson noise, to be

$$S_{\text{target}} = t_{\text{exp}} C_{\text{target}} \quad (1)$$

$$N_{\text{target}} = \sqrt{t_{\text{exp}} C_{\text{target}}} \quad (2)$$

where t_{exp} is the exposure time and C_{target} is the electrons per second from the target. In order to estimate the amount of defocussing required (the actual shape of the PSF does not enter these calculations), we distribute these equally over n_{pix} pixels by specifying a maximum number of electrons per pixel from the target and the background, m_{total} . Fig. 1 shows that this approach is imperfect so we also specify the maximum electrons per pixel from the target alone, m_{target} . This allows us to limit the *range* of counts within a structured PSF, and thus avoid saturating the most illuminated pixels.

If the sky background is low then we need only to account for the limit set by m_{target} in working out how many pixels to put the target electrons into:

$$n_{\text{pix}}(m_{\text{target}}) = \frac{S_{\text{target}}}{m_{\text{target}}} \quad (3)$$

If the sky background is high then we must increase the number of pixels containing counts from the target to avoid

⁷ Information on the Isaac Newton Group’s SIGNAL code can be found at <http://catserver.ing.iac.es/signal/>

broaching the m_{total} limit. In this case the number of pixels in the PSF is:

$$n_{\text{pix}}(m_{\text{total}}) = \frac{S_{\text{target}}}{m_{\text{total}} - C_{\text{sky}} t_{\text{exp}}} \quad (4)$$

where C_{sky} is the electrons per second per pixel from the sky background. For a specific situation, n_{pix} is taken to be the larger of the two alternatives.

Now we have found n_{pix} we can calculate the total sky level in the PSF, and the ensuing Poisson noise, in one observation:

$$S_{\text{sky}} = t_{\text{exp}} n_{\text{pix}} C_{\text{sky}} \quad (5)$$

$$N_{\text{sky}} = \sqrt{t_{\text{exp}} n_{\text{pix}} C_{\text{sky}}} \quad (6)$$

The contribution from CCD detector readout noise is:

$$N_{\text{ron}} = n_{\text{ron}} \sqrt{n_{\text{pix}}} \quad (7)$$

where n_{ron} is the readout noise per pixel in electrons.

The treatment of flat-field noise is more difficult, as the PSFs of one star in different observations will have many pixels in common whose flat-field noise will therefore cancel out. We approximate this noise contribution using f_{flat} , the flat-field noise per pixel (expressed as a fraction of the electrons in a pixel), and apply it to a number n_{flat} pixels where $n_{\text{flat}} \leq n_{\text{pix}}$. The flat-field noise is then

$$N_{\text{flat}} = f_{\text{flat}} \left(\frac{S_{\text{target}}}{n_{\text{pix}}} + C_{\text{sky}} \right) \frac{n_{\text{flat}}}{n_{\text{pix}}} \quad (8)$$

We can now express these noise levels as fractions of the total electrons from the star in magnitude units:

$$\sigma_{\text{target}} = -2.5 \log_{10} \left(\frac{S_{\text{target}} - N_{\text{target}}}{S_{\text{target}}} \right) \quad (9)$$

$$\sigma_{\text{sky}} = -2.5 \log_{10} \left(\frac{S_{\text{target}} - N_{\text{sky}}}{S_{\text{target}}} \right) \quad (10)$$

$$\sigma_{\text{ron}} = -2.5 \log_{10} \left(\frac{S_{\text{target}} - N_{\text{ron}}}{S_{\text{target}}} \right) \quad (11)$$

$$\sigma_{\text{flat}} = -2.5 \log_{10} \left(\frac{S_{\text{target}} - N_{\text{flat}}}{S_{\text{target}}} \right) \quad (12)$$

The noise due to scintillation can be found using the relation given by Dravins et al. (1998) and originally due to Young (1967):

$$\sigma_{\text{scint}} = 0.004 D^{-2/3} X^{7/4} e^{-h/H} (2t_{\text{exp}})^{-1/2} \quad (13)$$

where D is the telescope aperture (m), X is the airmass, h is the altitude of the telescope (m), and $H = 8000$ m is the scale height of the atmosphere. Note that scintillation varies seasonally, and the exponent of the airmass term actually varies between 1.5 and 2.0 depending on the direction of the wind relative to the telescope pointing (Dravins et al. 1998). These caveats illustrate the approximate nature of S/N calculations.

We now have five noise contributions which can be added in quadrature to reveal the total noise for one magnitude measurement in one observation:

$$\sigma_{\text{total}} = \sqrt{\sigma_{\text{target}}^2 + \sigma_{\text{sky}}^2 + \sigma_{\text{ron}}^2 + \sigma_{\text{flat}}^2 + \sigma_{\text{scint}}^2} \quad (14)$$

The ratio of noise to signal per unit time is then

$$\rho_{\text{total}} = \sigma_{\text{total}} \sqrt{t_{\text{exp}} + d_{\text{readout}}} \quad (15)$$

where d_{readout} is the total dead time per observation (normally dominated by the CCD readout time). In reality there will be additional noise in differential photometry due to measurement of the magnitude of the comparison star. We do not include this here as its contribution to the total noise can be driven to a much smaller value than for other sources by using many comparison stars.

Using the above formulae we have performed S/N calculations for the observations presented in this work. We adopted $m_{\text{target}} = 10\,000$, $M_{\text{total}} = 40\,000$, $n_{\text{ron}} = 4.0$, $X = 1.2$, and neglected flat-fielding noise. We set $d_{\text{readout}} = 91$ s to represent the first of our two observing sequences. The predicted σ_{total} for $t_{\text{exp}} = 120$ s is 0.54 mmag (dark time), as compared to the 0.50 mmag we actually achieved. This good agreement could be further improved by tinkering with the input parameters to the S/N calculations.

The resulting curves of noise level per observation and per minute are plotted as a function of t_{exp} in Fig. 4. The ‘sweet spots’ representing the lowest achievable noise level per minute (indicated by filled circles) occur at $t_{\text{exp}} = 565$ s (dark time), 310 s (grey) and 163 s (bright). Specifying a shorter readout time or fainter target star would shift the sweet spots towards smaller t_{exp} . The abrupt change of slope visible in Fig. 4 at $t_{\text{exp}} = 740$ s (bright time) occurs when the sky background becomes so high that the starlight has to be spread over extra pixels to avoid transgressing the m_{total} limit. Using these S/N calculations we find that, except for a target star which is very faint, defocussing is always the best approach.

The exposure times yielding the lowest noise per minute for the current situation are too long to sample the light variations through a transit of WASP-5 adequately, which is why used $t_{\text{exp}} \leq 120$ s. This is partly due to the long readout time of the DFOSC CCD: adopting $d_{\text{readout}} = 39$ s (appropriate for our second transit sequence) shortens the optimal exposure times to 371 s (dark), 203 s (grey) and 107 s (bright).

7 DISCUSSION AND CONCLUSIONS

We have presented high-precision light curves of two transits of the transiting extrasolar planetary system WASP-5, obtained by heavily defocussing the Danish 1.5 m telescope at ESO La Silla. The defocussing caused the telescope PSF to take an approximately annular shape of diameter 40 pixels (16''). Data reduction was undertaken using standard aperture photometry techniques. Debiassing and flat-fielding the raw CCD images improved the results but only by a small amount, probably due to the use of autoguiding to confine the stellar PSFs to the same pixels on each image. Our final light curves have a scatter around the best-fitting model of 0.50 mmag and 0.59 mmag for the two transits, observed in dark and grey time, respectively.

We have presented detailed signal to noise calculations for defocussed photometry, taking into account Poisson noise from the target and background, readout noise, scintillation, and flat-fielding noise. Application of the resulting formulae to the current case yields a predicted noise level of 0.54 mmag (dark time), which is in good agreement with the

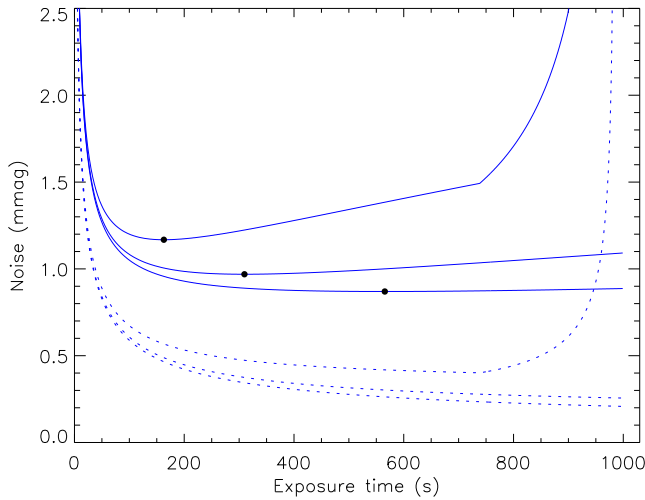


Figure 4. Predicted noise levels for the observations presented in this work, but as a function of exposure time. The dotted curves show the predicted noise level per observation for dark, grey and bright time (lower to upper curves). The solid curves show the predicted noise level per minute of telescope time (dark, grey, bright), and the optimum exposure times are indicated with filled circles.

actual values. We use these calculations to assess what exposure times would give the best overall signal to noise per unit time, finding 565 s (dark time) to 163 s (bright time). Such large values arise partly because of the long readout time of the DFOSC CCD, and are impractical because they would not properly sample the light variations through transit.

We find that telescope defocussing is a viable way of obtaining high-quality light curves of point sources over short periods of time. Its main advantages are that flat-fielding noise is averaged down and a smaller proportion of the observing time spent reading out the CCD. The scintillation and Poisson noise levels per unit time are ultimately limited by the telescope aperture rather than the observational strategy. One possible disadvantage of our approach is the use of a focal-reducing imager. These can be prone to internal reflections, which may have slightly increased the noise levels we find. One definite advantage, though, is that the telescope was equatorially mounted, so the target and comparison stars could be kept to the same light path whilst observing a transit. It is not possible to do this with altitude-azimuth telescopes, even if an image derotator is used, making such observations liable to problems with systematic errors.

The resulting light curves were modelled with the JKTEBOP code using the approach outlined by Southworth (2008). Limb darkening of the star was dealt with using five different LD laws, with similar results when one or both of the coefficients were included as parameters of the fit. We then adopted the observed T_{eff} , $\left[\frac{M}{H}\right]$ and velocity amplitude of the star (Anderson et al. 2008; Gillon et al. 2008b) and interpolated within the tabulated predictions of three different sets of theoretical stellar evolutionary models to derive the physical properties of the WASP-5 system (Southworth 2009). This approach has allowed us to assign both statistical and systematic errors to all output quantities. Our results are fully consistent with the homogeneous analyses of 14 tran-

siting extrasolar planetary systems presented by Southworth (2008, 2009).

We find that the planet WASP-5 b has a density equal to that of Jupiter, and that the system has an age of approximately 6 Gyr. The theoretical models presented by Fortney et al. (2007) can match WASP-5 b's mass and radius without requiring a heavy-element core. WASP-5 is also in line with the trend of planets with short orbital periods to have relatively high surface gravities (Southworth et al. 2007b) and masses (Mazeh et al. 2005). We calculate that its equilibrium temperature is $T_{\text{eq}} = 1732 \pm 80$ K, which may be high enough for WASP-5 b to fall into the 'pM class' of planets with large atmospheric opacities due to oxides of titanium and vanadium (Fortney et al. 2008). Its Safronov (1972) number is $\Theta = 0.0755 \pm 0.0096$, which makes it a Class II planet according to the study of Hansen & Barman (2007). However, Southworth (2009) found that the division between Class I and Class II objects is under threat from the steady addition of new discoveries to the catalogue of known transiting extrasolar planets, and may not be statistically significant. The high equilibrium temperature of WASP-5 b makes the system a good candidate for detecting the secondary eclipse at phase 0.5 (e.g. Deming et al. 2005; Harrington et al. 2007; Knutson et al. 2007), which would help our understanding of the physics of the atmospheres of gas giants. Such observations, as well as more precise measurements of the stellar velocity amplitude, T_{eff} and $\left[\frac{M}{H}\right]$, are encouraged.

ACKNOWLEDGMENTS

The photometric observations presented in this work will be made available at the CDS (<http://cdsweb.u-strasbg.fr/>) and at <http://www.astro.keele.ac.uk/~jkt/>.

We would like to thank the referee for a very useful report. JS acknowledges financial support from STFC in the form of a postdoctoral research assistant position. Astronomical research at the Armagh Observatory is funded by the Northern Ireland Department of Culture, Arts and Leisure (DCAL). VB, SCN, LM and GS acknowledge support by funds of Regione Campania, L.R. n.5/2002, year 2005 (run by Gaetano Scarpetta).

The following internet-based resources were used in research for this paper: the ESO Digitized Sky Survey; the NASA Astrophysics Data System; the SIMBAD database operated at CDS, Strasbourg, France; and the arXiv scientific paper preprint service operated by Cornell University.

REFERENCES

- Alonso, R., Barbieri, M., Rabus, M., Deeg, H. J., Belmonte, J. A., Almenara, J. M., 2008, *A&A*, 487, L5
- Anderson, D. R., et al., 2008, *MNRAS*, 387, L4
- Bakos, G., Noyes, R. W., Kovács, G., Stanek, K. Z., Sas-selov, D. D., Domsa, I., 2004, *PASP*, 116, 266
- Bruntt, H., Southworth, J., Torres, G., Penny, A. J., Clausen, J. V., Buzasi, D. L., 2006, *A&A*, 456, 651
- Charbonneau, D., Brown, T. M., Latham, D. W., Mayor, M., 2000, *ApJ*, 529, L45

- Christiansen, J. L., et al., 2008, in IAU Symposium 253, Transiting Planets, in press ([arXiv:0807.2852](#))
- Claret, A., 2000, *A&A*, 363, 1081
- Claret, A., 2004a, *A&A*, 428, 1001
- Claret, A., 2004b, *A&A*, 424, 919
- Claret, A., 2005, *A&A*, 440, 647
- Claret, A., 2006, *A&A*, 453, 769
- Claret, A., 2007, *A&A*, 467, 1389
- Claret, A., Hauschildt, P. H., 2003, *A&A*, 412, 241
- Clausen, J. V., 1998, in Kjeldsen, H., Bedding, T. R., eds., The First MONS Workshop: Science with a Small Space Telescope, p. 105
- Demarque, P., Woo, J.-H., Kim, Y.-C., Yi, S. K., 2004, *ApJS*, 155, 667
- Deming, D., Seager, S., Richardson, L. J., Harrington, J., 2005, *Nature*, 434, 740
- Demory, B.-O., et al., 2007, *A&A*, 475, 1125
- Dravins, D., Lindegren, L., Mezey, E., Young, A. T., 1998, *PASP*, 110, 610
- Etzel, P. B., 1981, in Carling, E. B., Kopal, Z., eds., Photometric and Spectroscopic Binary Systems, NATO ASI Ser. C., 69, Dordrecht, p. 111
- Fortney, J. J., Marley, M. S., Barnes, J. W., 2007, *ApJ*, 659, 1661
- Fortney, J. J., Lodders, K., Marley, M. S., Freedman, R. S., 2008, *ApJ*, 678, 1419
- Gilliland, R. L., et al., 1993, *AJ*, 106, 2441
- Gillon, M., Triaud, A. H. M. J., Mayor, M., Queloz, D., Udry, S., North, P., 2008a, *A&A*, 485, 871
- Gillon, M., et al., 2007, *A&A*, 472, L13
- Gillon, M., et al., 2008b, *A&A*, in press, [arXiv:0812.1998](#)
- Girardi, L., Bressan, A., Bertelli, G., Chiosi, C., 2000, *A&AS*, 141, 371
- Hansen, B. M. S., Barman, T., 2007, *ApJ*, 671, 861
- Harrington, J., Luszcz, S., Seager, S., Deming, D., Richardson, L. J., 2007, *Nature*, 447, 691
- Henry, G. W., Marcy, G. W., Butler, R. P., Vogt, S. S., 2000, *ApJ*, 529, L41
- Hoxie, D. T., 1973, *A&A*, 26, 437
- Jenkins, J. M., Caldwell, D. A., Borucki, W. J., 2002, *ApJ*, 564, 495
- Johnson, J. A., Winn, J. N., Cabrera, N. E., Carter, J. A., 2008, [arXiv:0812.0029](#)
- Knutson, H. A., et al., 2007, *Nature*, 447, 183
- Mayor, M., Queloz, D., 1995, *Nature*, 378, 355
- Mazeh, T., Zucker, S., Pont, F., 2005, *MNRAS*, 356, 955
- Nelson, B., Davis, W. D., 1972, *ApJ*, 174, 617
- Popper, D. M., Etzel, P. B., 1981, *AJ*, 86, 102
- Ribas, I., Morales, J. C., Jordi, C., Baraffe, I., Chabrier, G., Gallardo, J., 2008, *Memorie della Societa Astronomica Italiana*, 79, 562
- Safronov, V. S., 1972, *Evolution of the Protoplanetary Cloud and Formation of the Earth and Planets* (Jerusalem: Israel Program for Scientific Translation)
- Southworth, J., 2008, *MNRAS*, 386, 1644
- Southworth, J., 2009, *MNRAS*, in press, [arXiv:0811.3277](#)
- Southworth, J., Maxted, P. F. L., Smalley, B., 2004a, *MNRAS*, 349, 547
- Southworth, J., Maxted, P. F. L., Smalley, B., 2004b, *MNRAS*, 351, 1277
- Southworth, J., Maxted, P. F. L., Smalley, B., 2005a, *A&A*, 429, 645
- Southworth, J., Smalley, B., Maxted, P. F. L., Claret, A., Etzel, P. B., 2005b, *MNRAS*, 363, 529
- Southworth, J., Bruntt, H., Buzasi, D. L., 2007a, *A&A*, 467, 1215
- Southworth, J., Wheatley, P. J., Sams, G., 2007b, *MNRAS*, 379, L11
- Stetson, P. B., 1987, *PASP*, 99, 191
- Swain, M. R., Vasisht, G., Tinetti, G., 2008, *Nature*, 452, 329
- Tonry, J. L., Howell, S. B., Everett, M. E., Rodney, S. A., Willman, M., VanOutryve, C., 2005, *PASP*, 117, 281
- Torres, G., Ribas, I., 2002, *ApJ*, 567, 1140
- Udry, S., Santos, N. C., 2007, *ARA&A*, 45, 397
- Van Hamme, W., 1993, *AJ*, 106, 2096
- Winn, J. N., et al., 2007a, *AJ*, 133, 1828
- Winn, J. N., et al., 2007b, *AJ*, 134, 1707
- Young, A. T., 1967, *AJ*, 72, 747